Proceedings of the
Annual Stability Conference
Structural Stability Research Council
Baltimore, Maryland, April 10-13, 2018

Local buckling limit states in rod-braced metal building frames

Hamid. Foroughi[1], Chengda. Ji[2], Benjamin W. Schafer[3], Christopher D. Moen[4]

Abstract

Flange local buckling in metal building primary frames can initiate as rod brace anchor loads are carried through the closest steel frame flange to a girt, purlin, or to flange bracing collectors. Anchor rods are typically placed eccentrically in a steel frame, adjacent to one flange of the built-up steel cross-section to limit local web deformation, and this eccentricity initiates weak axis bending and torsion that is accompanied by axial force from the rod inclination. An experimental program was conducted to study frame-anchor interaction and document strength limit states. One of these limit states was flange local buckling, which resulted in a sudden primary frame lateral stiffness reduction that was mitigated after buckling by high warping restraint provided by frame continuity, leading to a stiff post-buckling path at large lateral frame deformations. The experimental results inspired a primary frame structural model, developed with insight from thin-shell finite element simulations, that allows mapping of rod anchor forces to flange demand, critical elastic buckling, and yielding parameters that define flange slenderness. With this model in hand, possible approaches for calculating metal building primary frame capacity including flange local buckling are explored, and possible pathways for future research are identified.

1. Introduction

The Metal Building Manufacturers Association (MBMA) invested in a research program to study ultimate strength limit states for rod-bracing lateral resisting systems, as shown in Fig. 1. The results of this study and exploration of the observed local buckling limit state are summarized in this paper.

[1] Graduate Research Assistant, Dept. of Civil Engineering, Johns Hopkins University, <hforoug1@jhu.edu>
[1] Graduate Research Assistant, Dept. of Mechanical Engineering, Johns Hopkins University, <cji7@jhu.edu>
[3] Professor, Dept. of Civil Engineering, Johns Hopkins University, <schafer@jhu.edu>
[4] Associate Research Professor, Dept. of Civil Engineering, Johns Hopkins University,<cmoen@jhu.edu>

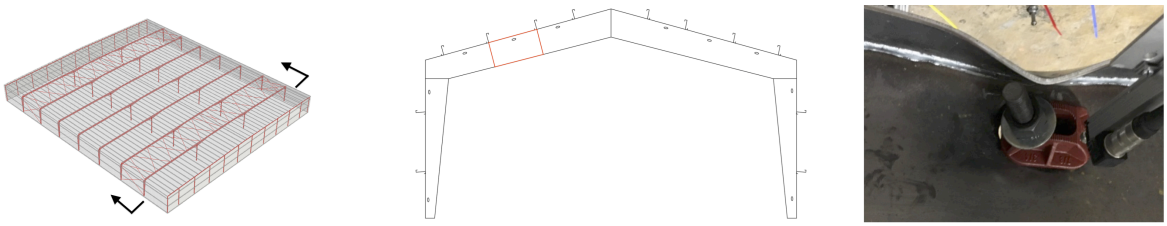

(a) (b) (c)

Figure 1: Rod bracing as a lateral system in a metal building: (a) bracing ties primary steel frames together in roof and walls (MBMA 2016); (b) rods are typically anchored near the top of a primary frame; (c) view from back of rod bracing anchorage location - local buckling deformation can develop if the primary frame flange is used to carry the rod brace force before it is taken out by flange bracing or girts or purlins

Metal building systems are interdependent assemblages of structural elements that work together to create an efficient structural system. The basic elements of the metal building system are primary steel frames, secondary purlin and girt members, and metal roof and wall cladding. Among various lateral load-resisting systems, rod-braced anchorage has been widely used in low-rise metal buildings (Sinno 1993). The tension force in the rod or cable brace can create a unique combination of weak axis bending and direct torsion in columns and rafters of the framing members, which are interconnected by purlins, girts and other girder members to form the building framework. Local buckling of the free flange closest to the anchor point (see Fig. 1c) may develop depending upon the built-up primary frame cross-sectional slenderness, and this limit state is challenging to predict because of the combination of warping torsion stresses, axial stresses from the inclined rod, and weak axis bending as the rod anchor reacts against the frame.

Local buckling prediction methods that treat complex stress states on cross-sectional elements like the free flange close to a rod anchor typically take one of two paths: (1) calculate the influence of each internal action separately and then use strength interaction equations; or (2) approximate the stress distribution on the cross-section, apply it as a reference stress in an elastic buckling analysis, and use this critical elastic buckling parameter to calculate slenderness and predict capacity. For interaction between internal forces and torsion, AISC 360-16 (AISC 2016) encourages this methodology, i.e., to calculate the elastic buckling loads from this interaction, and cap the strength at the load magnitude that creates first yield in the cross-section. The American Iron and Steel Institute Direct Strength Method (DSM) (AISI 2016) approach builds upon these ideas by calculating a local buckling slenderness considering the interactive stress state on the cross-section and including post-buckling capacity. The Direct Strength Method has been shown to be a viable approach for quantifying local buckling capacity of steel structural members (Seif and Schafer 2009; Seif and Schafer 2010).

The focus of this study is to propose possible approaches for an accurate local buckling prediction method considering the in-situ stress state developed in metal building primary frames tied together with rod anchors. The research is informed with an experimental program, introduced in the following section, and high fidelity simulations that provide valuable insight as primary frame local buckling deformation develops from bending stresses, direct torsion, and high warping restraint.

2. Rod-braced anchor experimental program

2.1 Experimental goals, test matrix, and specimen dimension nomenclature

A testing strategy was designed for MBMA to identify rod anchor limit states that extracts a portion of a primary frame (see red outline in Fig. 1b) and varies frame dimensions to initiate rod fracture, web bearing, and in some cases, local buckling limit states. Specimen groups are summarized in Table 1 with dimensional ranges specified by metal building manufacturers in an industry survey (Foroughi et al. 2018).

Specimen dimension nomenclature is defined in Fig. 2. The nominal web depth h=610 mm and oval anchor rod hole length and depth are L_{hole}=540 mm and w_{hole}=270 mm respectively. The rod anchor hole is located at the midlength of each specimen, with the hole centerline 508 mm from the bottom of the web plate. The length of the rod from hillside washer to the actuator is approximately L_{rod}=1150 mm. All specimens were fabricated with a one-sided fillet weld connecting flange and web plates, with the specimen oriented in the test frame such that the weld was on the same side as the hillside washer during loading. A minimum of three tests was performed for each configuration.

Table 1: Test matrix and nominal specimen dimensions

Specimen Group	Description	Rod angle	Specimen cross-section		
			Web	Flanges	
		θ	t_w	b_f	t_f
		degrees	mm	mm	mm
C	Control	45	4.8	152	6.4
W	Reduce web thickness	45	3.4	152	6.4
F	Increase flange width and thickness	45	4.8	203	13
A	Increase rod angle	60	4.8	152	6.4

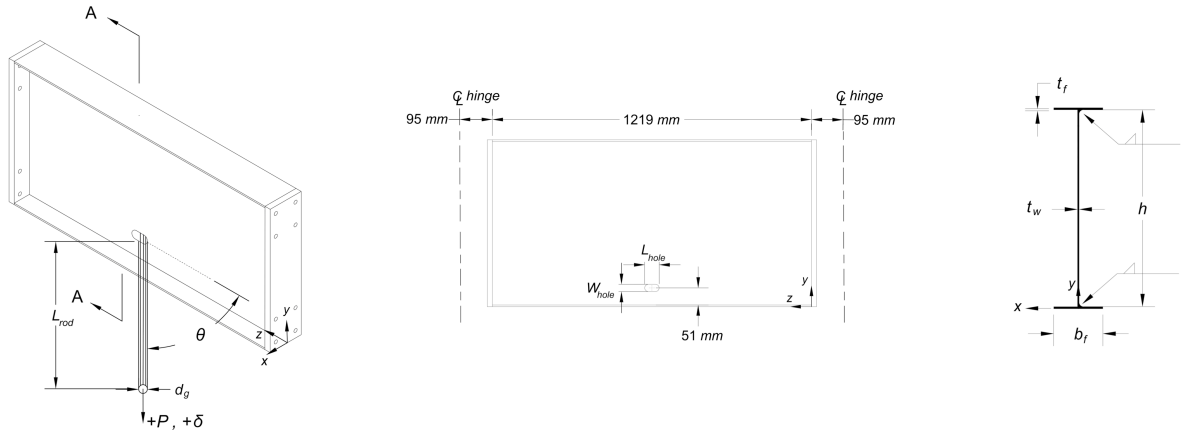

(a) Isometric (b) Elevation (c) Section A-A

Figure 2: Metal building primary frame steel plate girder specimen dimension nomenclature

2.2 Test setup

The test setup simulates an anchor rod engaging a metal building frame as lateral bracing. Clevis and pin connections are utilized at the specimen ends as shown in Fig. 1 creating boundary conditions with high warping restraint. The centerline pin-to-pin distance L=1409 mm. Framing orientation is flipped upside down compared to its position in a metal building (rod anchored in the bottom flange) to minimize eccentricity and deformation in the test frame. The anchor rods are produced with ASTM 1554-55 steel and they have a nominal outer unthreaded diameter of 220 mm. The mill certificates provided with the rods recorded their yield stress as 580 MPa.

Figure 3: Metal building primary frame test setup with rod anchor

2.3 Specimen loading and instrumentation

Each specimen was loaded with a hydraulic actuator at a displacement rate of 6 mm/minute. Rod load was recorded with a load cell attached to the actuator with an accuracy of +/- 0.4 kN and rod displacement was recorded with an internal actuator LVDT with an accuracy of +/- 0.3 mm. Additional measurements not discussed in this paper were made with position transducers (PTs) that allow the decomposition and study of local web deformation and rigid body rotation and twist, and those results are summarized in the MBMA final report (Foroughi et al. 2018). The maximum load expected in a test was the nominal tensile load of the rod, $P_{n,rod}$ =169 kN calculated as 580 MPa yield stress multiplied by the unthreaded rod area of 388 mm^2 and then reduced by 75% to account for fracture in the threaded plane consistent with AISC 360-16.

2.4 Specimen measurements and material properties

Cross-section dimensions were measured in each element – top flange, web, and bottom flange and the results are presented in Table 2 as an average of three measurements.

Table 2: Measured specimen dimensions

Specimen Name	Top Flange	Web	Bottom Flange
	b_f	h	b_f
	mm	*mm*	*mm*
C1	152	608	152
C2	152	608	152
C3	152	608	152
C4	152	608	152
W1	152	608	152
W2	152	611	152
W3	152	610	152
W4	152	610	152
F1	204	604	203
F2	204	608	203
F3	204	608	204
F4	204	608	204
A1	152	609	151
A2	152	609	152
A3	152	609	152

Tensile coupon tests were performed in accordance with ASTM E8/E8M-16 (ASTM 2016) on the plate used to manufacture the specimens – 2 web plates and 2 flange plates if different thicknesses. Plates of the same thickness were sourced from the same heat. Average steel yield stress σ_y, steel ultimate stress σ_u, and percent elongation at σ_u are summarized in Table 3.

Table 3. Specimen steel yield stress, ultimate stress, and elongation

Specimen name	Flanges					Web				
	t_f	w_{coupon}	σ_y	σ_u	elongation at σ_u	t_w	w_{coupon}	σ_y	σ_u	elongation at σ_u
	mm	mm	MPa	MPa	%	*mm*	mm	MPa	MPa	%
C1	6.3	12.7	492	552	18	4.6	12.6	411	500	25
C2	6.2	12.7	492	552	18	4.6	12.6	411	500	25
C3	6.4	12.7	492	552	18	4.6	12.6	411	500	25
C4	6.4	12.7	492	552	18	4.6	12.6	411	500	25
W1	6.2	12.7	492	552	18	3.4	12.5	332	508	31
W2	6.1	12.7	492	552	18	3.4	12.5	332	508	31
W3	6.2	12.7	492	552	18	3.4	12.5	332	508	31
W4	6.2	12.7	492	552	18	3.4	12.5	332	508	31
F1	12.9	12.6	364	579	34	4.6	12.6	411	500	25
F2	12.9	12.6	364	579	34	4.6	12.6	411	500	25
F3	13.1	12.6	364	579	34	4.6	12.6	411	500	25
F4	13.1	12.6	364	579	34	4.6	12.6	411	500	25
A1	6.5	12.7	492	552	18	4.6	12.6	411	500	25
A2	6.1	12.7	492	552	18	4.6	12.6	411	500	25
A3	6.3	12.7	492	552	18	4.6	12.6	411	500	25

2.4 Rod anchor load-deformation response results

Load-deformation trends for the specimen groups are provided in Fig. 4 to 7. Initial nonlinearity at small loads resolved as the hillside washer settled into bearing against the web. Localized web deformation continued up to $0.40P_{n,rod}$ with linear pre-peak stiffness that varied as a function of built-up cross-section dimensions; for example, compare 2190 kN/m for the control group C to 4105 kN/m for the increased flange width and thickness group F. Flange local buckling deformation initiated in all specimens except those in the F group (a wider, thicker flange) with a typical buckling half-wave shown in Fig. 8 developing slightly offset from the centerline, see Table 4 for measured half-wavelength L_{cr} and offset from the half-wave centerline from the centerline of the anchor web hole, $\Delta z_{,cr}$ where $+z$ is defined in Fig. 2. The flange local bucking caused stiffness degradation and rapid out-of-plane anchor deflection and rotation that terminated when high warping restraint provided by the test boundary conditions engaged. The warping restraint reestablished anchor stiffness and load increased until either rod failure or local web bearing failure. All tests ended when the hillside washer nipple slipped off the web bearing point except for test C2 where the rod fractured.

Table 4. Flange local buckling test load, measured half-wavelength and half-wave offset from centerline anchor

	Test measurements			Thin-shell finite element eigen-buckling analysis		
Specimen Name	Rod load at buckling in test	Buckling half-wavelength	Half-wave offset from anchor location	Critical elastic flange local buckling load	Buckling half-wavelength	Half-wave offset from anchor location
	$P_{test,FLB}$ kN	$L_{cr,test}$ mm	$\Delta z_{cr,test}$ mm	$P_{cr,FLB}$ kN	L_{cr} mm	Δz_{cr} mm
C1	82.8	137	5	271	120	13
C2	83.6	132	15	271	120	13
C3	79.2	140	20	271	120	13
C4	77.4	135	5	271	120	13
W1	79.0	161	15	253	134	25
W2	75.6	153	5	253	134	25
W3	79.4	156	15	253	134	25
W4	74.8	161	10	253	134	25
F1	No Buckling	No Buckling	No Buckling	2014	230	26
F2	No Buckling	No Buckling	No Buckling	2014	230	26
F3	No Buckling	No Buckling	No Buckling	2014	230	26
F4	No Buckling	No Buckling	No Buckling	2014	230	26
A1	60.0	122	5	242	112	15
A2	65.0	120	5	242	111	15
A3	66.3	125	5	242	110	15

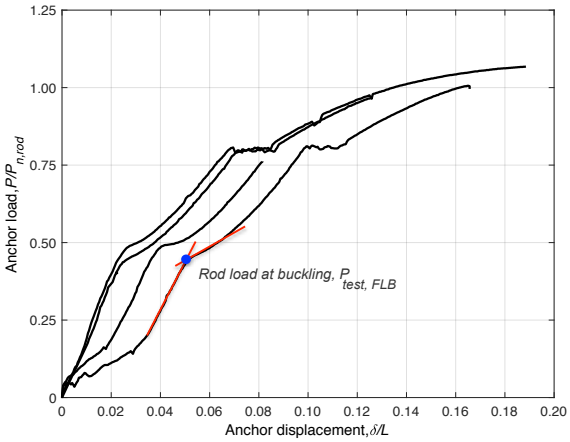

Figure 4: Test group C (control) load-deformation response

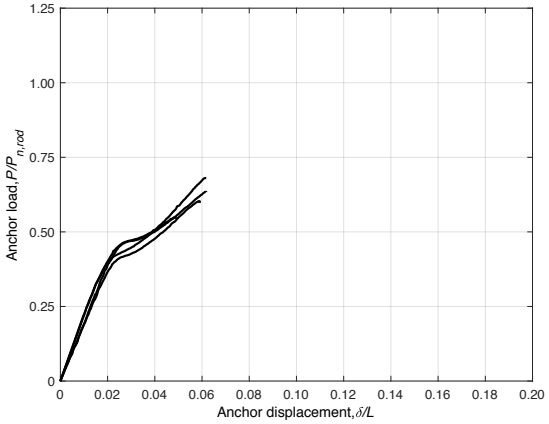

Figure 5: Test group W (reduced web thickness) load-deformation response

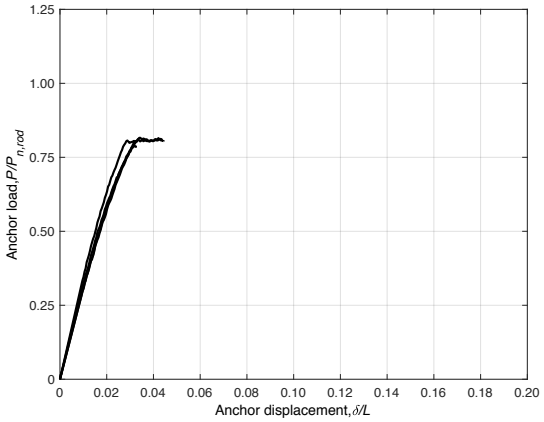

Figure 6: Test group F (increased flange width and thickness) load-deformation response

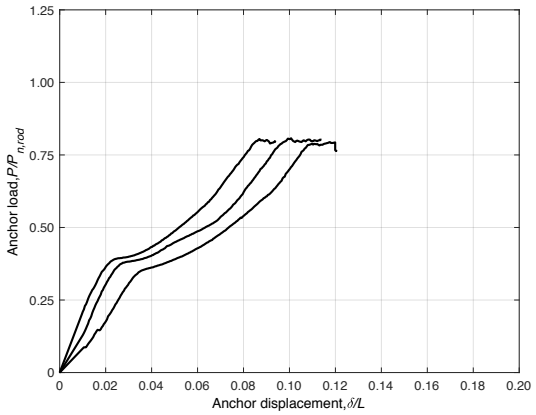

Figure 7: Test group A (decreased rod angle) load-deformation response

Figure 8: Typical flange local buckling deformation (W1 test shown)

The rod load at which flange local buckling initiated, $P_{test,FLB}$, is summarized in Table 4, calculated at the intersection of the pre-buckling and post-buckling slopes as annotated in Fig. 4. The buckling loads observed in the test are used to explore possible buckling limit state prediction approaches in the following section.

3. Flange local buckling limit state in rod-braced metal building frames

Flange local buckling is a strength limit state that should be considered for rod braced lateral systems if the flange adjacent to the anchor is expected to carry the rod brace force to a collector, e.g., flange bracing or purlins or girts. The stress gradient evolution in the flange adjacent to the anchor is challenging to predict because of the high warping restraint and because of local web-flange deformation. The first step is to identity the reference stress that should be considering in the local buckling prediction.

3.1 Elastic buckling modes from thin-shell finite element eigen-buckling analysis

Thin-shell finite element models of the tested specimens were constructed in the commercial finite element program ABAQUS (Simulia 2018) as part of the larger MBMA research program. The models simulate the clevis-pin boundary conditions and include the geometry of the hillside washer (modeled as solid elements) and rod as they engage the primary frame web. Model details and comparisons of simulation to the tested load-deformation results are provided in Foroughi et. al (2018).

This verified model capability is a powerful tool for studying flange local buckling. For example, an eigen-buckling analysis of each specimen type in a group (C, W, F, and A) leads to a critical elastic buckling load that includes the pre-buckling stress state in the flange from localized shear, weak axis flexure, and warping torsion stresses. A typical elastic buckling mode shape for the control specimen group is provided in Fig. 9 and $P_{cr,FLB}$, L_{cr}, and $\Delta_{z,cr}$ are summarized in Table 4. The buckled mode shape is short enough to develop between girts and purlins and adjacent to discrete flange bracing typically designed in metal buildings to limit lateral-torsional buckling. Observe in Table 4 that L_{cr} and $\Delta z,_{cr}$ are consistent with test measurements, and that $P_{cr,test}$ is lower than $P_{cr,FLB}$ because local deformation and yielding at the web-flange junction, along with manufacturing imperfections - web bow relative to the flanges and canted flanges as documented in Foroughi et al. (2018), trigger buckling earlier than the elastic bifurcation load.

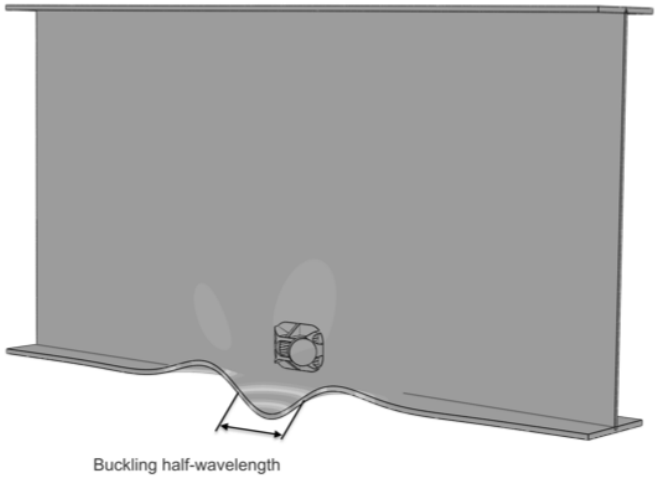

Figure 9: Flange local buckling mode shape from thin-shell finite element eigen-buckling analysis (Group C specimen shown)

3.2 Flange stress evolution that leads to local buckling deformation

The specimen finite element models can also be used to follow the stress gradient evolution in the built-up girder flange adjacent to the anchor that results in local buckling. The longitudinal stress gradient (stress in the z-direction, σ_z, as defined in Fig. 2) at the flange midplane for the control series (C group) of experiments is shown in Fig. 10 for rod loads from $0.13P_{n,rod}$ (about 22 kN) to the tested buckling load $P_{test,FLB}$=$0.48P_{n,rod}$ (about 80 kN). The stress gradient remains

linear, with slight deviations when approaching $P_{cr,test}$. Typically in an unstiffened element, the midplane stresses reach yield near the supported edge and drop off towards the free edge because out-of-plane plate buckling deformation is highest (and in-plane plate stiffness is lowest). This particular case is different because the high warping restraint boundary conditions limit buckling deformation and allowing the flange to carry load after buckling.

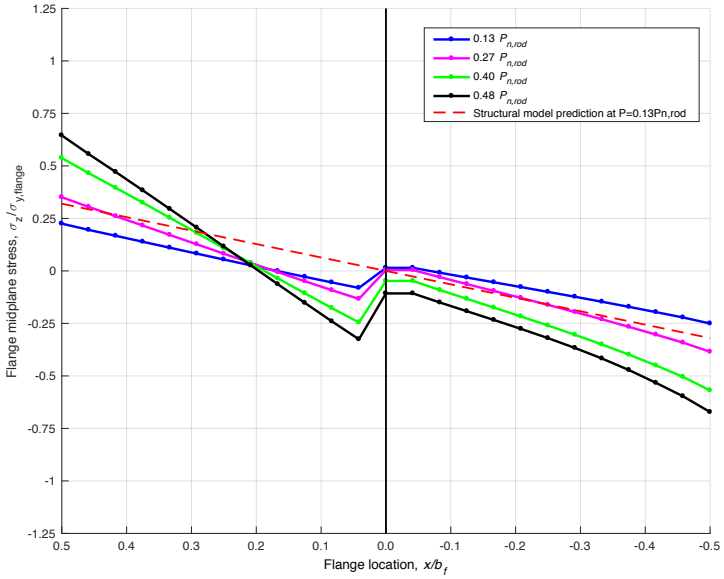

Figure 10: Flange longitudinal midplane stress evolution with applied rod anchor load for C (control) specimen, $+x$ is tension side, $-x$ is compression (buckling) side

The flange stresses in Fig. 10 are not readily calculated by decomposing the applied rod force into x and z vector components and summing the stresses from the resulting axial force, weak axis moment and a direct torsion. This is because the plate girder cross-section does not act as a rigid element, and instead local deformation dominates. The web bends out-of-plane locally at the anchor in the experiments, and the flange closest to the anchor displacing relative to the other flange resulting in web double curvature.

A simplified structural model shown in Fig. 11 of this case is proposed, where the x-portion of the anchor load ($P\sin\theta$) is applied to the flange and where the web is simulated as a distributed lateral spring. A frame element analysis shown in Fig. 12 using MASTAN2 (Ziemian 2009) for each specimen group. For the Control specimen flange adjacent to the anchor, springs representing y-direction restraint to the flange k_y=12EI/h^3=9.53E-5 kN/mm/mm where I=1/12(1)t_w^3, and pinned warping-free end conditions. The analysis reveals a nonlinear moment gradient in the specimen flange and localized deformation at the application of load in Fig. 12.

It is useful to compare flange stresses predicted by the structural model in Fig. 11 to those from thin-shell FEA in Fig. 10. The flange tip stress developed in the structural model at a load P=0.13$P_{n,rod}$ is 0.32$\sigma_{y,flange}$ which is higher but comparable to 0.25$\sigma_{y,flange}$ in Fig. 10. The model boundary conditions could be made more consistent with those in a primary frame without much effort – considering semi-rigid flexural connections, for example.

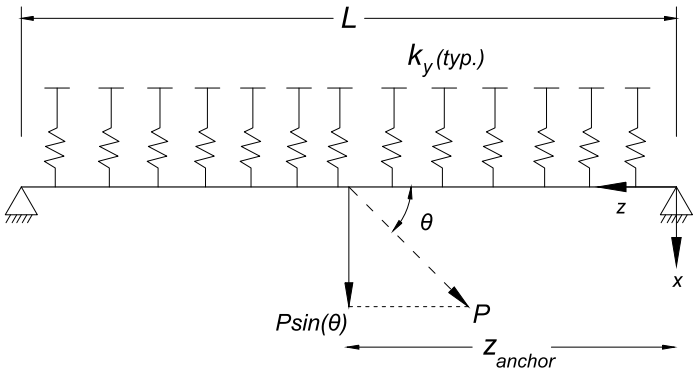

Figure 11: Structural model for a rod anchor located adjacent to a primary frame flange

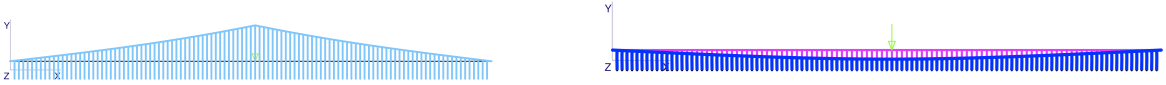

Moment diagram

Displaced shape

Figure 12: Flange moment and displaced shape for a C group specimen from MASTAN2 structural model

The structural model is useful because (1) it provides a convenient way of calculating the pre-buckling reference flange stress; (2) it provides the anchor load that causes first yield in the flange; and (3) it is an accessible method (in lieu of thin-shell FEA) to approximate the demand on the flange for metal building engineers. In the experimental program, the rod load is assumed to be applied halfway between girt or purlin brace force collectors. The rod load P could be moved to a different location (a different z_{anchor}, see Fig. 11) in the structural model and the resulting flange tip demand stress would be less for the same rod brace load, reflecting the case where local buckling might not control. A classical beam on an elastic foundation model could work here as well to provide a closed-formed solution for flange moment instead of using computer structural analysis.

3.3 Calculation of critical elastic flange local buckling load with the structural model

The flange critical elastic buckling load is calculated using the finite strip eigen-buckling program CUFSM (Schafer 2018) with the assumed reference stress distribution on the flange adjacent to the rod calculated by applying a reference rod load P=1 kN on the frame structural model in Fig. 11, obtaining the resulting flange moment (M=181.4 kN-mm), and calculating the flexural stress with $\sigma_z = My/I_f$ (flange tip stress is 7.4 MPa when P=1 kN) where $I_f = 1/12 t_f b_f^3$. The reference stress distribution and resulting buckled mode shape from CUFSM is shown in Fig. 13 for the C specimen group, and $P_{cr,CUFSM}$=221 kN. The thin-shell eigen-buckling load, $P_{cr,FEM}$=270 kN (see Table 5) is 20% higher than that predicted by the structural model because warping restraint, pre-buckling stress distributions, and cross-section connectivity are taken into account more accurately. The CUFSM half-wavelength L_{cr}=152 mm is also consistent with $L_{cr,test}$ and L_{cr} from thin-shell finite element eigen-buckling analysis, see Table 4. The flange

yield load $P_{y,flange}$ is calculated with the structural model in Fig. 11 by increasing P until the flange moment causes first yield. For the Control specimen group, the yield flange moment M_y=12094 kN-mm for a rod load P=66.6 kN at σ_y=492 MPa.

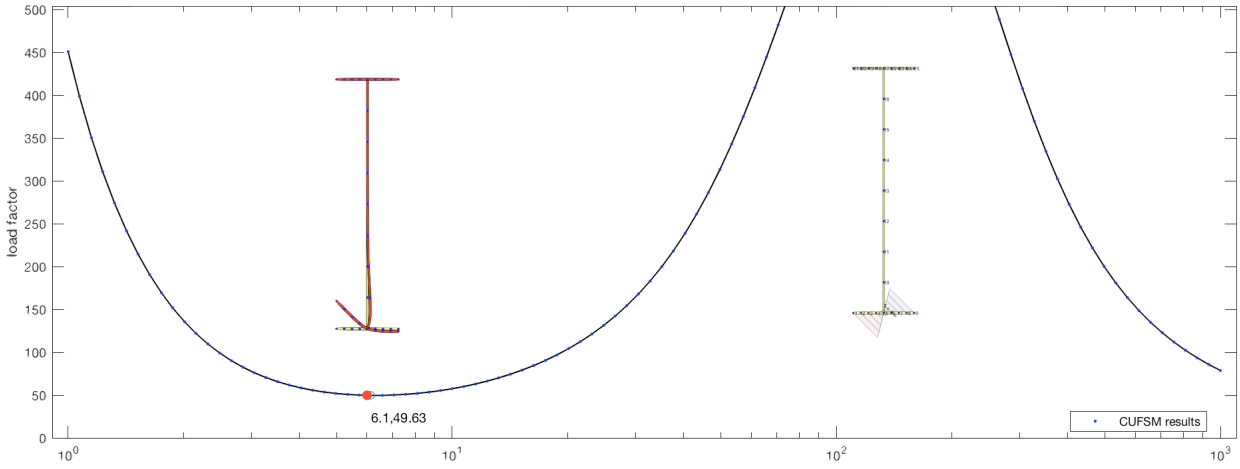

Figure 13: CUFSM finite strip elastic buckling analysis for flange local buckling (C specimen group shown) with reference stress for the case of a rod anchored adjacent to a flange

3.4 Possible future paths for developing a flange local buckling prediction method

The AISC strength prediction method (AISC 360-16, Section F6) considering flange local buckling for I-sections bent about their weak axis is not applicable to the case here of a localized force at an eccentricity in the web. Another path through the AISC provisions is to use Section H3, subsection 3 for non-HSS members in torsion and combined stress where the local buckling strength is limited to the critical elastic buckling load considering the combine actions (e.g., the CUFSM analysis shown in Fig. 13), calculated by analysis (F_n=F_{cr}), and capped by the load that causes first yield anywhere in the cross-section (F_n=F_y).

It is shown in Table 5 that the tested buckling loads are closest in magnitude to the anchor rod load that causes yielding in the flange tip, and that elastic buckling on its own is not a good predictors of flange local buckling capacity. It is hypothesized that local web deformation causes flange rotation and an out-of-plane imperfection with increasing load that initiate the buckling deformation observed in the tests. The framework for a possible local buckling prediction method emerges from this study, however more research is needed to understand how local web-flange rotation at the anchor initiates flange local buckling.

Table 5. Tested flange local buckling loads, elastic buckling and yield parameters

Specimen Name	Tested Buckling Strength	Elastic Buckling and Yielding		
	$P_{cr,test}$ kN	$P_{cr,\ FEA}$ kN	$P_{cr,\ CUFSM}$ kN	$P_{y,\ str\ model}$ kN
C1	82.8	270.5	221.0	66.6
C2	83.6	270.5	221.0	66.6
C3	79.2	270.5	221.0	66.6
C4	77.4	270.5	221.0	66.6
W1	79	252.2	221.0	66.6
W2	75.6	252.2	221.0	66.6
W3	79.4	252.2	221.0	66.6
W4	74.8	252.2	221.0	66.6
F1	No Buckling	1890.5	1625.7	175.2
F2	No Buckling	1890.5	1625.7	175.2
F3	No Buckling	1890.5	1625.7	175.2
F4	No Buckling	1890.5	1625.7	175.2
A1	60	260.3	180.2	54.3
A2	65	260.3	180.2	54.3
A3	66.3	260.3	180.2	54.3

4. Conclusion

Flange local buckling can develop in metal building primary frames when rod brace anchor forces are carried through the frame flanges. The resulting stresses in the cross-section are highly influenced by local web deformation at the anchorage and by the flexibility of the web which allows the flange closest to the anchor to displace laterally. With high warping restraint, the resulting midplane flange stresses that develop from the eccentric rod load can be calculated with an approximate structural model of just the flange adjacent to the rod anchor considering the web as a lateral spring and including any other bracing points (girts, purlins). This model opens up the possibility for flange local buckling strength prediction if the influence of local web-flange rotation on buckling can be better understood and studied in future work.

Acknowledgments

The authors are grateful to the Metal Building Manufacturers Association for its funding support and to the MBMA Project Monitoring Task Group for their thoughtful guidance throughout the project. We are also indebted to Nick Logvinovsky, manager of the Thin-Walled Structures Lab at Johns Hopkins University, who supported the experimental program.

References

Sinno, R. R. (1993). "X-Bracing Anchorage Connection." *Journal of Structural Engineering,* 119(11) 3360-3383.

Foroughi, H., Ji, C., Schafer, B.W., Moen, C.D. (2018). "Strength and Stiffness of Metal Building Rod Brace Anchorage Connections." *Cold-Formed Steel Research Symposium (CFSRC) Final Report to the Metal Building Manufacturers Association*, Cleveland, OH.

Ziemian, R.D., McGuire, W. (2009). "MASTAN2 version 3.2", www.mastan2.com.

Abaqus, Simulia. (2011). "Dassault Systemes." Providence, RI, USA.

Schafer, B.W., Ádány, A. (2006). "Buckling analysis of cold-formed steel members using CUFSM: conventional and constrained finite strip methods." *Eighteenth international specialty conference on cold-formed steel structures.*

American Iron and Steel Institute (AISI) (2016). "North American Specification for the Design of Cold-formed Steel Structural Members." S100-12.

Seif, M., Schafer, B.W. (2010). "Local buckling of structural steel shapes." *Journal of Constructional Steel Research,* 66(10), 1232-1247.

Seif, M., Schafer, B.W. (2009). "Elastic buckling finite strip analysis of the AISC sections database and proposed local plate buckling coefficients." *Structures Congress 2009: Don't Mess with Structural Engineers: Expanding Our Role,* 1-10.

Schafer. B.W. (2018). "CUFSM 5, elastic buckling analysis of thin-walled members by finite strip analysis".

AISC (2016). "Specification for Structural Steel Buildings. ANSI/AISC 360-16." *American Institute of Steel Construction*, Chicago, IL.

ASTM, (2009). "Standard Test Methods for Tension Testing of Metallic Materials. ASTM E8/E8M." *American Society for Testing and Materials*, West Conshohocken, PA, USA.